Oscillations, criticality and responsiveness in complex brain networks

MinKyung Kim[1,2] and UnCheol Lee[1,2]

Corresponding author: UnCheol Lee (uclee@umich.edu)

[1]Department of Anesthesiology, University of Michigan Medical School, Ann Arbor, MI 48109, USA

[2]Center for Consciousness Science, University of Michigan Medical School, Domino's Farms, P.O. Box 385, Ann Arbor, MI 48105, USA

Abstract

Brain networks during unconscious states resulting from sleep, anesthesia, or traumatic injuries are associated with a limited capacity for complex responses to stimulation. Even during the conscious resting state, responsiveness to stimulus is highly dependent on spontaneous brain activities. Many empirical findings have been suggested that the brain responsiveness is determined mainly by the ongoing brain activity when a stimulus is given. However, there has been no systematic study exploring how such various brain activities with high or low synchronization, amplitude, and phase response to stimuli. In this model study, we simulated large-scale brain network dynamics in three brain states (below, near, and above the critical state) and investigated a relationship between ongoing oscillation properties and a stimulus decomposing the brain activity into fundamental oscillation properties (instantaneous global synchronization, amplitude, and phase). We identified specific stimulation conditions that produce varying levels of brain responsiveness. When a single pulsatile stimulus was applied to globally desynchronized low amplitude of oscillation, the network generated a large response. By contrast, when a stimulus was applied to specific phases of oscillation that were globally synchronized with high amplitude activity, the response was inhibited. This study proposes the oscillatory conditions to induce specific stimulation outcomes in the brain that can be systematically derived from networked oscillator properties, and reveals the presence of state-dependent temporal windows for optimal brain stimulation. The identified relationship will help advance understanding of the small/large responsiveness of the brain in different states of consciousness and suggest state-dependent methods to modulate responsiveness.

Author Summary

A responsiveness of the brain network to external stimulus is different across brain states such as wakefulness, sleep, anesthesia, and traumatic injuries. It has been shown that responsiveness of the brain during conscious state also varies due to the diverse transient states of the brain characterized by different global and local oscillation properties. In this computational model study using large-scale brain network, we hypothesized that the brain responsiveness is determined by the interactions of networked oscillators when a stimulus is applied to the brain. We examined relationships between responsiveness of the brain network, global synchronization levels, and instantaneous oscillation properties such as amplitude and phase in different brain states. We found specific stimulation conditions of the brain that produce large or small levels of responsiveness. The identified relationship suggests the existence of temporal windows that periodically inhibit sensory information processing during conscious state and develops state-dependent methods to modulate brain responsiveness considering dynamically changed functional brain network.

Introduction

The brain's responsiveness to external stimuli significantly depends on the overall brain state and is dramatically restricted in unconscious states resulting from sleep, general anesthesia, or traumatic injuries. Previous studies with transcranial magnetic stimulation (TMS) have demonstrated that the effects of stimulation during sleep (NREM), anesthesia, and vegetative states are simple and constrained to local areas, whereas more complex, diffuse responses are typically found during the conscious state [1–4]. Furthermore, in the state of wakefulness, the brain's response to stimuli has also been associated with oscillation properties, such as amplitude and phase, at the moment when the stimulus is applied. In visual perception tasks, for example,

target detectability is dependent on the power and phase of ongoing alpha waves (~10Hz) [5–14]. Recent repetitive TMS (rTMS) studies have suggested that the instantaneous phase of sensorimotor μ-rhythm in the α band (8-12Hz) is an important determinant of stimulation efficacy [15,16].

Although a link between these oscillation properties and responsiveness has been suggested, there has been no systematic exploration of how a stimulus interacts with spontaneous brain activity and results in state-specific outcomes. In this paper, we hypothesized that the brain responsiveness is determined largely by the networked oscillation properties when a stimulus is applied to the brain. To test this hypothesis, we constructed a large-scale brain network dynamics using coupled oscillator model (Stuart-Landau) based on anatomically informed human brain network structure. In the model, three brain states were defined with modulating the criticality (below, near, and above critical state), which produces various networked oscillations in the brain network (large or small synchronization, amplitude, and phase). Here, we simulated alpha oscillations (~10Hz) that have been successfully simulated by simple coupled oscillators, and examined how well the characteristic responsiveness of various oscillations explains the observed empirical results without implementing details of state-specific neurophysiology. The alpha oscillation models have been successfully explained empirically observed brain network behaviors such as functional connectivity, traveling waves, and network state transitions in the electroencephalography (EEG), magnetoencephalography (MEG), and functional MRI (fMRI), which indicates that alpha oscillations may be fit well to study the responsiveness of the brain network [17–24]. To the best of our knowledge, the response behaviors of various alpha oscillations in the brain network have not been studied.

In the model, the critical state was defined as the state with the largest metastability, a measure of the variance of synchronization fluctuation across time [25]. When a system is near its critical

point, i.e., the balanced state between order and disorder, the largest fluctuation in dynamics is observed [26,27]. During the conscious resting state in the brain, the dynamics are near the critical point and marked by large fluctuations in synchrony [28,29]. Notably, disruptions to the resting state (e.g., sleep, anesthesia, traumatic injuries) appear to mitigate the fluctuation variance by causing a transition away from criticality [30].

Here we decomposed various brain activities into fundamental oscillation properties: (large/small) instantaneous global synchronization, amplitude, and phase, modulating the criticality (below, near, and above critical states) and investigated a relationship between oscillation properties and a stimulus. We found specific oscillation properties that induce large/small responsiveness, which is also consistent with the empirical observations for the presence of rhythmic temporal windows of large/small responsiveness to a stimulus [5,6,31–34]. Our model study may provide a theoretical framework to interpret complex responses of the brain in different states of consciousness in terms of fundamental networked oscillation properties. In the following result sections, we first show that the characteristics of the three brain states and the oscillation properties at the stimulus onset. Second, we demonstrate distinct response behaviors of the amplitude and phase synchronization to the pulsatile stimulus across states. Thus, we quantify the changes of both amplitude and phase synchronization as responsiveness indexes. Next, we show how the instantaneous global synchronization level correlates with the responsiveness of amplitude and phase synchronization with different responsiveness measures. Specific phases of alpha oscillations that induce large or small responsiveness are also demonstrated. Finally, we compare the responsiveness of the regional stimulation with effective, random, and non-effective stimulation conditions we identified in the model study. A schematic diagram of the study design is presented in Fig 1.

Fig 1. Schematic diagram of the study design. In this study, we simulated alpha oscillations using coupled Stuart-Landau model on the human brain network structure that consists of 82 brain regions. The brain states were classified into below, near, and above critical states based on their global synchronization level and the metastability (the variance of synchronization fluctuation). The critical state C_p was defined as the state with the largest metastability. A global pulsatile stimulus was applied to various ongoing alpha oscillations in the three brain states. We then quantified a perturbation response of amplitude (PR_j^{amp}) and a phase synchronization (PR_j^{sync}) for node j after the stimulus onset (j=1, 2, …,82), in a binary fashion. To measure responsiveness to the stimulus, we first defined responsivity R_j, as the temporal average of PR_j^{amp} (PR_j^{sync}) during 600 msec (200 msec). Second, Lempel-Ziv complexity (LZc) of PR_j^{amp} (PR_j^{sync}) was calculated to measure the perturbational complexity of the brain's response to the applied stimulus. In doing so, we identified a relationship between the ongoing brain state and the degree of responsiveness and identified the effective stimulus conditions for inducing a large response. Finally, we applied the stimulus to the occipital region and compared the performance between the effective and random stimulation conditions.

Results

The characteristics of alpha oscillations for the three brain states

To study a relationship between oscillation properties at the stimulus onset and the responsiveness, we simulated networked alpha oscillations of the 82 brain regions using coupled Stuart-Landau model in three different brain states, $\mathrm{C_b}$, $\mathrm{C_p}$, and $\mathrm{C_a}$ (see Materials and methods for details). The alpha oscillations demonstrated various oscillation properties across states in terms of variance of instantaneous synchronization, instantaneous synchronization and amplitude. Figure 2A demonstrates the metastability of alpha oscillations in the three brain states, which defined as the variance of instantaneous global synchronization level $\mathrm{r(t)}$ over time. The alpha oscillations at $\mathrm{C_p}$ show significantly large variances of $\mathrm{r(t)}$ compared to those of $\mathrm{C_b}$ and $\mathrm{C_a}$. Fig 2B and C demonstrate distinct oscillation properties of the three brain states at the stimulus onsets. The alpha oscillations at $\mathrm{C_p}$ have a balanced distribution of $\mathrm{r(t)}$ in the middle of the two extreme cases. The distributions of $\mathrm{r(t)}$ at $\mathrm{C_b}$ and $\mathrm{C_a}$ are characterized by small and large $\mathrm{r(t)}$, respectively

(Fig 2B). The $\mathrm{r(t)}$ values at the stimulus onsets are 0.26 $\pm$ 0.04 (Mean $\pm$ SD) for $\mathrm{C_b}$, 0.45 $\pm$ 0.11 for $\mathrm{C_p}$ and 0.75 $\pm$ 0.08 for $\mathrm{C_a}$. The amplitudes of the alpha oscillations of $\mathrm{C_p}$ have a broad and balanced distribution, however, the alpha oscillations of $\mathrm{C_b}$ and $\mathrm{C_a}$ show narrow/relatively small amplitudes and broad/biased distribution toward large amplitude, respectively (Fig 2C). The amplitudes at the stimulus onsets are 1 $\pm$ 0.01 for $\mathrm{C_b}$, 1.2 $\pm$ 0.07 for $\mathrm{C_p}$ and 1.83 $\pm$ 0.08 for $\mathrm{C_a}$ (Mean $\pm$ SD). To simplify our model, we applied a simple form of stimulus (pulsatile) to all nodes for 50 msec, which enables us to exclude the effects of stimulus type and network structure (i.e., hub and periphery) in our consideration. Total 500 stimulation trials were performed for each state.

Fig 2. The characteristics of alpha oscillations in the three brain states, C_b C_p, and C_a and instantaneous oscillation properties at the stimulus onset for each state. (A) Mean and variance (metastability) of instantaneous global synchronization $r(t)$ for C_b (blue), C_p (red), and C_a (yellow). The critical state C_p is characterized by the largest metastability (Mean $\pm$ SD = 0.01 $\pm$ 0.005), compared to smaller metastability values of C_b and C_a. (B) Distributions of instantaneous global synchronization $r(t)$ at the stimulus onset for C_b (blue), C_p (red), and C_a (yellow). Total 500 stimulation trials were performed for each state. The $r(t)$ values at C_b and C_a are characterized by small and large averages of $r(t)$, respectively. The $r(t)$ at C_p is balanced in the middle of the two extreme cases. (C) Node amplitude distributions at stimulus onset for C_b, C_P, and C_a. The amplitudes of alpha oscillations at C_b and C_a are biased with smaller and larger amplitudes, while the amplitudes at C_p are relatively unbiased. These characteristic and state-specific alpha oscillations may result in distinct responses to the stimulus.

Distinct responses of amplitude and phase synchronization

The effects of a stimulus at differing levels of global synchronization, amplitude, and phase of the alpha oscillations across three distinct brain states, $\mathrm{C_b}$, $\mathrm{C_p}$, and $\mathrm{C_a}$, were investigated. Perturbation responses (PRs) of amplitude ($\mathrm{PR_j^{amp}(t)}$) and phase synchronization ($\mathrm{PR_j^{sync}(t)}$) of a node j (j = 1, 2, …, 82) at time t were defined as 1 if the change was significant, otherwise, as 0 (see Materials

and methods for details). Fig 3B and C present examples of $\mathrm{PR}_{\mathrm{j}}^{\mathrm{amp}}$ and $\mathrm{PR}_{\mathrm{j}}^{\mathrm{sync}}$. The black dots represent $\mathrm{PR}_{\mathrm{j}}^{\mathrm{amp}}$ ($\mathrm{PR}_{\mathrm{j}}^{\mathrm{sync}}$) equal to 1 after the stimulation. We investigated the temporal properties of average $\mathrm{PR}_{\mathrm{j}}^{\mathrm{amp}}$ and $\mathrm{PR}_{\mathrm{j}}^{\mathrm{sync}}$ over nodes for the three brain states. The results from 500 stimulus applications across each brain state was divided into five groups, classified by the level of $\mathrm{r(t)}$. We found distinct response durations of amplitude and phase synchronization following the stimulation. Notably, $\mathrm{PR}^{\mathrm{amp}}$ persisted significantly longer than $\mathrm{PR}^{\mathrm{sync}}$ ($p<0.001$, sign test, $\mathrm{PR}^{\mathrm{amp}} > \mathrm{PR}^{\mathrm{sync}}$ after 100ms for all $\mathrm{C_b}$, $\mathrm{C_p}$, and $\mathrm{C_a}$). For instance, at $\mathrm{C_b}$ the $\mathrm{PR}^{\mathrm{amp}}$ was maintained for approximately 800 msec, whereas the $\mathrm{PR}^{\mathrm{sync}}$ diminished before 200 msec. The longer persistence of $\mathrm{PR}^{\mathrm{amp}}$ was observed in all three states. This implies that amplitude and phase synchronization in the brain network are governed by distinct response mechanisms, which might be associated with distinct temporal dynamics of amplitude and phase synchronization in the resting state [35]. We tested differing stimulus strengths (p=10, 20, 30, 40, and 50) as well as stimulus durations (50,100,150, 200, 250 msec) at $\mathrm{C_p}$ (S1 Fig and S2 Fig). From the following analyses, we quantify the changes of both amplitude and phase synchronization as responsiveness indexes separately setting different durations (600 and 200 msec).

Fig 3. Distinct perturbation responses (PRs) of amplitude and phase synchronization. (A) Examples of global synchronization fluctuations for the three brain states, C_b, C_p, and C_a. Each black triangle indicates the stimulus timing of one trial. PRs of (B) amplitude (PR^{amp}) and (C) phase synchronization (PR^{sync}) are presented as examples of one stimulation trial. The stimulus was applied at time zero. A red shaded area indicates the stimulus duration (= 50 msec). The black dots of each node indicate the time points at which the stimulus induces significantly increased amplitude (phase synchronization); PR_j^{amp} (PR_j^{sync}) = 1. Average (D) PR^{amp} and (E) PR^{sync} over all nodes for the trials with different instantaneous global synchronization levels r(t) are compared, respectively. The instantaneous global synchronization levels were divided into five groups: q(0)-q(20), q(20)-q(40), q(40)-q(60), q(60)-q(80), and q(80)-q(100) regarding the % quantiles. The lines with shaded regions indicate the mean $\pm$ standard error. PR^{amp} and PR^{sync} are differentiable, that is, the PR^{amp} maintains longer than the PR^{sync}.

Correlation between responsivity and instantaneous global synchronization level

We investigated the relationship between instantaneous global synchronization level $\mathrm{r(t)}$ and the responsivity of amplitude and phase synchronization, respectively. The responsivity $\mathrm{R}_{\mathrm{j}}^{amp}$ ($\mathrm{R}_{\mathrm{j}}^{sync}$) measures the total amount of $\mathrm{PR}_{j}^{\mathrm{amp}}$ ($\mathrm{PR}_{\mathrm{j}}^{sync}$), defined as a significant change of amplitude (phase synchronization) of node j within the epoch (600 msec for $\mathrm{R}^{\mathrm{amp}}$ and 200 msec for $\mathrm{R}^{\mathrm{sync}}$) following the stimulus. The epoch was determined to cover the maximum persistence of each responsivity in our simulation. The average responsivity for $<\mathrm{R}^{\mathrm{amp}}>$ and $<\mathrm{R}^{\mathrm{sync}}>$ was calculated by taking the average of $\mathrm{R}_{\mathrm{j}}^{\mathrm{amp}}$ and $\mathrm{R}_{\mathrm{j}}^{\mathrm{sync}}$ over all nodes in order to investigate the relationship with the global feature $\mathrm{r(t)}$. The $<\mathrm{R}^{\mathrm{amp}}>$ and $<\mathrm{R}^{\mathrm{sync}}>$ for $\mathrm{C_b}$, $\mathrm{C_p}$, and $\mathrm{C_a}$ are presented with respect to $\mathrm{r(t)}$ in Fig 4A and 4B. Both $<\mathrm{R}^{\mathrm{amp}}>$ and $<\mathrm{R}^{\mathrm{sync}}>$ at $\mathrm{C_b}$ (incoherent state) are larger than those of the other states with small variances (Mean $\pm$ SD: 0.7 ± 0.05 for $<\mathrm{R}^{\mathrm{amp}}>$ and 0.62 ± 0.03 for $<\mathrm{R}^{\mathrm{sync}}>$). By contrast, the responsivity at $\mathrm{C_a}$ (highly synchronized state) is diverse, with a relatively larger r(t) overall. Spearman correlations between $\mathrm{r(t)}$ and the $<\mathrm{R}^{\mathrm{amp}}>$ and $<\mathrm{R}^{\mathrm{sync}}>$ are presented in Fig 4C & 4D. At $\mathrm{C_p}$, both $<\mathrm{R}^{\mathrm{amp}}>$ and $<\mathrm{R}^{\mathrm{sync}}>$ are significantly correlated with the $\mathrm{r(t)}$ (Spearman correlations: $\rho^{\mathrm{R}^{\mathrm{amp}}} = -0.33, \mathrm{p} < 0.001$ for $<\mathrm{R}^{\mathrm{amp}}>$; $\rho^{\mathrm{R}^{\mathrm{sync}}} = -0.53, \mathrm{p} < 0.001$ for $<\mathrm{R}^{\mathrm{sync}}>$). At $\mathrm{C_p}$, a globally desynchronized state showed larger responsivity for both amplitude and phase synchronization to the stimulus, whereas at the brain states far from the critical state, $\mathrm{C_b}$and $\mathrm{C_a}$, the responsivities were not highly correlated with the $\mathrm{r(t)}$.

Fig 4. Correlations between instantaneous global synchronization level $r(t)$ and the responsivity of amplitude (R^{amp}) and phase synchronization (R^{sync}). The average responsivity of (A) amplitude and (B) phase synchronization for 500 stimulation trials is presented with respect to r(t) for the three brain states, C_b (blue), C_p (red), and C_a (yellow). Spearman correlations between r(t) and the global (C) amplitude

responsivity, $\rho^{R^{amp}}$, and (D) synchronization responsivity, $\rho^{R^{sync}}$, for C_b (blue), C_p (red), and C_a (yellow) are presented. ***p<0.001 and **p<0.01. At C_p, applying the stimulus at smaller r(t) induces larger R^{amp} and R^{sync}.

Correlation between perturbational Lempel-Ziv complexity and instantaneous global synchronization level

We investigated the relationship between instantaneous global synchronization level $\mathrm{r(t)}$ and the perturbational complexities of amplitude and phase synchronization. We calculated the Lempel-Ziv Complexity (LZc) [36] of the $\mathrm{PR^{amp}}$ ($\mathrm{PR^{sync}}$) in response to the stimulus, which served as the measure of perturbational complexity. LZc of the PR is similar to the Perturbational Complexity Index (PCI), a measure that has been previously applied to experimental data with demonstrably good performance for distinguishing consciousness from sleep, anesthesia, and pathologic unconsciousness [2,4]. In the same way with $<\mathrm{R^{amp}}>$ and $<\mathrm{R^{sync}}>$, we first calculated the LZc of each node with $\mathrm{PR^{amp}_j}$ and $\mathrm{PR^{sync}_j}$ (binary patterns) for their associated epochs (600 msec and 200 msec, respectively), and calculated the average over 82 nodes defining $<\mathrm{LZc^{amp}}>$ and $<\mathrm{LZc^{sync}}>$. Fig 5A and 5B present $<\mathrm{LZc^{amp}}>$ and $<\mathrm{LZc^{sync}}>$ with respect to $\mathrm{r(t)}$ for the three brain states ($\mathrm{C_b}$, $\mathrm{C_p}$, and $\mathrm{C_a}$), and show the results of 500 stimulus trials for each state. Among the three states, $\mathrm{C_p}$ has large $<\mathrm{LZc^{amp}}>$ and $<\mathrm{LZc^{sync}}>$ (See S3 Fig.), indicating that the largest flexibility and responsiveness of the brain network occurred at the critical state for both amplitude and phase synchronization. Spearman correlations between $\mathrm{r(t)}$ and $<\mathrm{LZc^{amp}}>$ and $<\mathrm{LZc^{sync}}>$ were presented in Fig 5C & 5D. At $\mathrm{C_p}$, a globally desynchronized state showed larger perturbational complexities for both amplitude and phase synchronization to the stimulus. The $<\mathrm{LZc^{amp}}>$ at $\mathrm{C_p}$ showed a small correlation with r(t) ($\rho^{LZc^{amp}} = -0.14$, $^{**}p < 0.01$), by contrast, $<\mathrm{LZc^{sync}}>$ at $\mathrm{C_p}$ is significantly correlated with $\mathrm{r(t)}$ ($\rho^{LZc^{sync}} = -0.60$, $^{***}p < 0.001$). The result

implies that, within the critical state, stimulation during desynchronized alpha oscillations induces more complex perturbation patterns in phase synchronization.

Fig 5. Correlations between instantaneous global synchronization level r(t) and the perturbational Lempel-Ziv Complexity (LZc) for the amplitude ($\boldsymbol{LZc^{amp}}$) and the phase synchronization ($\boldsymbol{LZc^{sync}}$). The average (A) LZc^{amp} and (B) LZc^{sync} for 500 stimulus trials is presented with respect to the r(t) for C_b (blue), C_p (red), and C_a (yellow). Spearman correlations between r(t) and (C) the average LZc^{amp}, $\rho^{LZc^{amp}}$ and (D) the average LZc^{sync}, $\rho^{LZc^{sync}}$ are presented for C_b (blue), C_p (red), and C_a (yellow), respectively. **p<0.01 and ***p<0.001 for the Spearman correlation value. At C_p, applying stimulus at lower level of instantaneous global synchronization induces larger perturbational complexities for both amplitude and phase synchronization.

Specific phases of alpha oscillations with inhibited response to external stimuli

We expanded the investigation to explore the amplitude and phase dependencies across different levels of responsiveness ($\mathrm{R^{amp}}$, $\mathrm{R^{sync}}$, $\mathrm{LZc^{amp}}$, and $\mathrm{LZc^{sync}}$) at $\mathrm{C_p}$. We first classified the alpha oscillation properties at the stimulus onset in $\mathrm{C_p}$ into four groups based on the instantaneous global synchronization level (high/low) and amplitude (high/low). Nodes were first classified by determining whether the observed instantaneous global synchronization was higher (HS) or lower (LS) relative to the average instantaneous global synchronization across 500 stimulus trials. This same approach was used to further classify the nodes via their measured amplitude (HA/LA) relative to the average amplitude. We found that the responsiveness of LS & LA (red line) is larger than that of HS & HA (blue line) in most phases (See black lines in Fig 6, p<0.005, Wilcoxon rank-sum test). Interestingly, stimulating at specific phases from 60° to 180° of HS & HA shows significantly smaller responsiveness, which is consistent in four different measures ($\mathrm{R^{amp}}$, $\mathrm{R^{sync}}$, $\mathrm{LZc^{amp}}$, and $\mathrm{LZc^{sync}}$) (Fig 6A-D). By contrast, the synchronization responsiveness ($\mathrm{R^{sync}}$ and

LZc^{sync}) of LS & LA have no phase dependence (Fig 6B and 6D). The results suggest that the existence of periodic temporal windows (phases from 60° to 180 in each cycle of alpha wave) that create network conditions of small responsiveness to external stimuli. The results for LS & HA and HS & LA are presented in S4 Fig. Different stimulus strengths at C_p were also tested (S5 Fig – S8 Fig). The results for the two other states, C_b and C_a are shown in S9 Fig and S10 Fig. As expected, the strength of stimulus significantly affects the phase dependence at C_p. A strong stimulus (larger than p=40 in S8 Fig.) begins to induce large changes in both amplitude and phase synchronization diminishing the phase dependence (p=50 in S9 Fig). On the contrary, a weak stimulus (p=10, S5 Fig.) produces small changes in amplitude and phase synchronization, thus, the phase dependences are indistinctive across the conditions (LS&LA, LS&HA, HS&LA, and HS&HA).

Fig 6. Specific alpha phases with inhibited response to the stimulus at C_p. For each panel, a red (blue) thick line indicates the average (A) R^{amp}, (B) R^{sync}, (C) LZc^{amp}, (D) LZc^{sync} of nodes with lower (higher) levels of instantaneous global synchronization and lower (higher) amplitude at the stimulus onset. Lower and higher levels of instantaneous global synchronization (amplitude) were distinguished by the average of instantaneous global synchronization levels of all trials (amplitudes of all nodes). Phases of nodes at the stimulus onset were sorted in 30 phase bins. Thin colored lines indicate the standard errors of responsiveness. Black lines present phase ranges with significantly different responsiveness between LS & LA and HS & HA ($p<0.005$, Wilcoxon rank-sum test). Lower levels of global synchronization and amplitude (LS & LA) show larger responsiveness to the stimulus than higher levels of global synchronization and amplitude (HS & HA) in most phases. Notably, for HS & HA, stimulation applied at specific phases of alpha waves from 60° to 180° showed lower responsiveness, implying the existence of temporal windows during which there is little response to external stimuli.

Stimulation of occipital region with effective, random, and non-effective conditions

We tested if the effective stimulation conditions identified in the global stimulation also hold for a local stimulation. Here we applied a stimulus to nodes within the radius of 50 mm centered a left cuneus in the occipital region at C_p (13 regions; (left) cuneus, inferior parietal, isthmus cingulate, lateral occipital, lingual, pericalcarine, precuneus, superior parietal, (right) cuneus, isthmus cingulate, lingual, pericalcarine, precuneus) to roughly simulate a stimulation to visual area, and compared four responsiveness measures, R^{amp}, R^{sync}, LZc^{amp}, and LZc^{sync}, of effective, non-effective, and random stimulation conditions. For the effective stimulation, we applied a stimulus during phases from 240° to 360° of alpha oscillations with a low level of instantaneous global synchronization and low amplitude (Fig 7). For the random stimulation, we applied a stimulus to random instantaneous states that may correspond to conventional stimulation methods. For the non-effective stimulation, we stimulated at phases from 60° to 180° of alpha oscillation with a high level of instantaneous global synchronization and high amplitude. We found that the effective (non-effective) stimulation conditions induce larger (smaller) responsiveness for R^{amap}, R^{sync}, LZc^{sync} (Fig 7A, 7B, and 7D). The random stimulation conditions were in the middle of two conditions. The responsiveness of the three conditions was significantly different in R^{amap}, R^{sync}, and LZc^{sync} (Kruskal-Wallis test, $p<0.001$) and a multi-comparison test was performed using the Tukey-Kramer method (*$p<0.05$ and ***$p<0.001$). However, since LZc^{amp} for the global stimulus was barely correlated with the instantaneous global synchronization ($\rho^{LZc^{amp}} = -0.14$ in Fig 5C), and not significantly distinguishable with the amplitude and phase (Fig 6C), LZc^{amp} for the local stimulus also showed relatively small values and can't be differentiated the three stimulation conditions. The results demonstrated that the effective and non-effective stimulation conditions we found in the global stimulation can be also applied to the local stimulation.

Fig 7. Comparison of the responsiveness due to a local stimulation with effective, random, and non-effective stimulation conditions. Average (A) R^{amp}, (B) R^{sync}, (C) LZc^{amp}, and (D) LZc^{sync} were calculated with three different conditions found in the global stimulation; (effective stimulation condition): alpha phases from 240° to 360° with low level of instantaneous global synchronization and low amplitude (red). (random stimulation condition): random selection from all stimulation trials (gray). (non-effective stimulation condition): alpha phases from 60° to 180° with high level of instantaneous global synchronization and high amplitude (blue). Effective (non-effective) stimulation conditions show a larger (smaller) responsiveness for R^{amp}, R^{sync},and LZc^{sync}. The results of three conditions are significantly different for R^{amp}, R^{sync}, LZc^{sync} (Kruskal-Wallis test, $p<0.001$). Multiple comparison test was performed with the Tukey-Kramer method (*$p<0.05$ and ***$p<0.001$).

Discussion

Many empirical studies have reported that the brain responsiveness to a stimulus is dependent upon brain state and ongoing spontaneous brain activities. Here, we hypothesized that the empirically observed response behaviors of the brain is determined by the interaction way of networked oscillators to a stimulus. To test the hypothesis, we used a human brain network model of coupled oscillators and decomposed the networked oscillations into fundamental oscillation properties (instantaneous global synchronization, amplitude, and phase) within the three brain states (C_b, C_p, and C_a). Each state presents characteristic oscillation features: (below the critical state, C_b) a low amplitude and incoherent state, (near the critical point, C_p) balanced high and low amplitudes with a large synchronization fluctuation, and (above the critical point, C_a) a high amplitude and highly synchronized state. How such characteristic oscillations respond to a stimulus provides a theoretical framework to understand the periodic temporal windows of

346 large/small responsiveness in conscious resting state as well as the distinct responsiveness of
347 the brain in different states of consciousness.

348 **Dependence on the criticality of the network**: Empirical and computational model studies have
349 proposed that the brain during conscious resting state resides near the critical state, whereas the
350 brain states under significant alterations such as anesthesia and traumatic injuries are distant
351 from the critical state [28–30,37]. In this model study, we observed that the amplitude responsivity
352 (; the amount of significantly increased amplitudes) at C_b and C_a was larger than that at C_p(Fig 4A).
353 However, the perturbational complexities of amplitude (; the temporal complexity of significantly
354 increased amplitudes) at C_b and C_a were smaller than C_p. The brain network at C_p exhibits the
355 largest perturbational complexity of the amplitude (Fig 5A and S3 Fig A). The amplitude
356 responsiveness is similar with the TMS outcomes in empirical studies. The TMS-evoked activities
357 during unconsciousness showed high-amplitude and short-lasting simple response patterns [1,3],
358 whereas the EEG responses induced by TMS in the resting state showed more complex
359 perturbational patterns compared to anesthesia and NREM sleep [1–4]. The similarity between
360 the model and the empirical results proposes that the state-dependent responses of the human
361 brain to TMS may be due to the distinct response behaviors of the characteristic states
362 (synchronous/incoherent or high/low amplitudes) of networked oscillators at below, near, and
363 above critical state.

364 **Dependence on the instantaneous global synchronization**: In the model, we found—even
365 assuming criticality—that the brain network responsiveness correlates with the level of
366 instantaneous global synchronization at the critical state. Lower levels of instantaneous global
367 synchronization produced larger responses for both amplitude and phase synchronization,
368 whereas higher levels of instantaneous global synchronization induced smaller responses.
369 Considering the large synchronization fluctuations over time at the critical state, it is important for

370 a stimulus to be applied at the appropriate time in order to induce a larger responsiveness.
371 Applying a stimulus without consideration of this relationship may in turn produce greater
372 variability in the stimulation outcomes. In addition, finding the dependence on instantaneous
373 global synchronization also provides a novel insight on the role of synchronization fluctuation for
374 the information processing in the brain. In the epochs with lower levels of instantaneous
375 synchronization, the brain might not be able to integrate distributed information within the brain
376 network, however, the brain can be highly susceptible to external stimuli. On the contrary, in the
377 epochs of higher levels of instantaneous synchronization, the brain might easily integrate
378 distributed information within the brain network, but the brain might not be able to respond to
379 external stimuli. Regarding the large synchronization fluctuation at critical state, the response
380 behavior of a network at high/low level of instantaneous synchronization seems to create temporal
381 windows that can integrate internal or external information separately, which may prevent mixing
382 of internal and external information in the brain.

383 **Dependence on the amplitude and phase of oscillation**: In our model study, we found that the
384 responsiveness correlates to the amplitude and phase of ongoing alpha oscillations. We
385 decomposed the alpha waves into high/low instantaneous synchronization levels, high/low
386 amplitudes and phases (0° to 360°). The responsiveness of lower instantaneous synchronization
387 level & low amplitude (LS & LA) was larger than that of higher instantaneous synchronization level
388 & high amplitude (HS & HA), irrespective to the phases (Fig 6). Importantly, considering the alpha
389 oscillations of high synchronization and high amplitude, we found that there are specific phases
390 (60° to 180°) exihibiting significantly lower responsiveness regardless of the responsiveness
391 measures. The results suggest another periodic temporal windows (phases from 60° to 180 in
392 each cycle of alpha wave) with inhibited response to external stimuli. The time scale of this
393 temporal window is much smaller than the time scales of synchronization fluctuations.

The amplitude and phase dependences have been observed in empirical studies. The amplitude and phase of the alpha waves (8-13Hz) are associated with the processing of sensory stimuli, especially in regards to visual perception [5–14]. Stimulation at lower amplitudes, and at phase near the trough of alpha waves, showed increased target detectability [6,8,10,11,13,38]. Phosphenes artificially induced by TMS were more detectable in lower pre-stimulus alpha power and specific alpha phase ranges [7,12,39]. Recent TMS studies also showed that a motor-evoked potential (MEP) amplitude is dependent on the pre-stimulus cortical μ-rhythm phase [15,16]. The established dependences on the amplitude and specific phases of alpha waves were consistent regardless of the stimulus types. Our human brain network model showed that stimuli applied at specific phases of alpha waves resulted in larger responsivity and perturbational complexity for both amplitude and phase synchronization at the critical state. Interestingly, the phase dependence was more pronounced when the stimulus was given at higher amplitudes of alpha oscillations, which is supported by the visual target detectability experiment [10]. This result emphasizes the importance of considering the effective stimulation conditions, especially when the stimulus is applied to the alpha waves with high amplitude and high levels of synchronization.

We also tested if the conditions identified from the global stimulation still hold for a local stimulation. We applied the same stimulus to the occipital region across three different conditions: effective (low instantaneous synchronization level, low amplitude, and phases of 240°-360°), non-effective (high instantaneous synchronization level, high amplitude, and phases of 60°-180°), and random (the conventional stimulation ways without considering ongoing brain activity). Relative to the random condition, the effective and non-effective conditions produced significantly larger and smaller brain responsiveness, respectively. These results may explain why the brain stimulation outcomes in conventional studies show such large inter-or intra-subject variability [40], which has affected the reliability and consistency of previous brain stimulation studies. In addition, finding the specific phases of the alpha oscillations for large or small responsiveness re-illuminates the

historical concept of the “neuronic shutter” described in 1960s [34], which implied the existence of temporal windows that periodically prohibit sensory information processing during conscious state [5,31–34,41,42]. Further study is required to identify a relevance of the temporal windows of sensory information processing to the response behavior of networked alpha oscillations to external stimuli.

Multi-scale mechanisms of large and small responsiveness: A desynchronized EEG, as characterized by low amplitude, noisy, and fast-frequency activity, is associated with arousal and increased awareness [43]. This desynchronized state emerges as the product of highly recurrent and stochastic interactions within, and between, the excitatory-inhibitory neuronal populations at both the cellular and network level [43]. At the cellular level, the stochastic interplay of excitatory and inhibitory conductance sets neurons into a high-conductance state with enhanced responsiveness. At the population level, neuronal ensembles also become highly responsive to afferent inputs [43]. At the large-scale brain network level, the responsiveness is determined with the characteristics of ongoing networked oscillators. However, it still remains to be answered how the specific oscillation properties induce such large or small responsiveness. One of the candidates to answer the question is the phase response curve (PRC) which has been studying in physics. The PRC characterizes the way that a system with a collective periodic behavior responds to external stimuli. The response of a periodically driven oscillating system to the stimuli is measured by the phase shift from the original phase. The ongoing phase value dependence of the phase shift (advancing or delaying the original phase) at which a stimulus occurs is an inherent characteristic of any oscillatory systems. This method has been applying to many rhythmic biological systems such as circadian rhythms, cardiac rhythms, and spiking neuron to study how external stimuli perturb the original rhythms [44–46]. The previous analytic studies discovered the influential factors causing phase shift and phase synchronization perturbation: a low (high) phase coherence induces a large (small) phase shift [45]. Stimulation to the phases around stable fixed

point of the PRC increases phase coherence, whereas stimulation to the phases around unstable fixed point decreases phase coherence. These properties also hold for networks with different coupling functions, network structure, connectivity, and even for amplitude dynamics of Stuart-Landau oscillators [47]. Our network model of alpha oscillations can be a complex real world example of the simple PRC models that constrained by the hierarchical human brain network connections. If the alpha oscillations possess globally coupled in the human brain network, the response behavior of alpha oscillations should be governed by the same mechanism. A stability analysis will be required to identify specific conditions of the human brain network that induce large or small responsiveness. Furthermore, the future study will be needed to establish how responsiveness across multiple scales, cellular, neural population, and large-scale brain network, are related to each other.

In summary, this model study demonstrated for the first time the relationship between network responsiveness to a stimulus and the decomposed oscillation properties at different network states (below, near, and above critical state). We found that brain states with lower levels of instantaneous global synchronization, lower amplitude, and specific phase ranges as well as a criticality, are important factors to consider for inducing greater network responsiveness. This study proposes systematically derived oscillatory conditions to induce specific stimulation outcomes in the brain network. The identified relationship will help advance understanding of the brain in states of small/large responsiveness and suggest methods by which to modulate responsiveness.

Limitations: This model study has some limitations. First, our model simulated only alpha oscillations. We assumed that the alpha oscillations are globally networked in the human brain because many global features of alpha oscillations such as functional connectivity, traveling waves, and network state transitions in empirical findings were successfully reproduced with

coupled oscillators of alpha frequency [17–24]. It also well fits to study the response behaviors of the human brain network due to previous empirical findings [5–14]. Second, we only tested a pulsatile stimulus. Despite the fact that we examined various strengths and durations of the pulsatile stimulus, we cannot assure whether other types of stimulus, for instance, continuous sinusoidal stimulus, gives the same result. Third, we applied a stimulus to all the nodes in the brain network and later tested only the occipital stimulation in order to simplify the model study. However, regarding the significant influence of network topology to local brain dynamics, it requires to identify the effect of stimulation sites on the responsiveness.

Material and Methods

Simulation of networked alpha oscillations in human brain network

We constructed a large-scale functional brain network using coupled Stuart-Landau models on the human anatomical brain structure to generate spontaneous oscillations. The Stuart-Landau model with brain topology has been used to replicate the oscillatory dynamics of different types of electromagnetic brain signals such as electroencephalography (EEG), magnetoencephalography (MEG) and functional magnetic resonance imaging (fMRI) [17,18,20,24,48]. The coupled Stuart-Landau model is defined as following:

$$\dot{z}_j(t) = \left\{\lambda_j + i\omega_j - |z_j(t)|^2\right\} z_j(t) + A_{ij}\sum_{k=1}^{N} K_{jk} z_k(t) - \tau_{jk} + \beta\xi_j(t) \qquad (1)$$

Here, the state of j_{th} oscillator, $j = 1,2,\ldots,N$, is determined by a complex variable $z_j(t)$ at time t. N is the total number of brain regions acquired from group-averaged diffusion tensor imaging (DTI) with 82 nodes [49]. The $A_{jk} = 1$ if there is a connection between j_{th} and k_{th} oscillators, and $A_{jk} = 0$ if there is not, based on the structural brain network. Each node undergoes supercritical Hopf

bifurcation and the dynamics of the oscillator settles on a limit cycle if $\lambda_j > 0$, and on a stable focus if $\lambda_j < 0$. Here, we fixed all λ_j as 1. The $\omega_j = 2\pi f_j$, is an initial angular natural frequency of each j_{th} oscillator. We used a Gaussian distribution for the f_j with the mean 10 Hz and standard deviation 0.5 Hz to simulate the alpha bandwidth of human EEG activity [20–22,24]. We also used homogeneous coupling term $K_{jk} = K$ between j_{th} and k_{th} oscillator from 0 to 0.4 with $\delta K = 0.002$ which determines the global connection strength among brain regions. The time delay between oscillators $\tau_{jk} = D_{jk}/s$ was introduced with the average speed of axons in brain areas, $s = 7\ ms$ [50], and the distance D_{jk} between brain regions. The node j received the input from connected nodes k after the time τ_{jk}. The time delays are various, but as long as the time delay is smaller than a quarter of the period of oscillators, here $\tau_{jk} < \sim 25ms$, results are not qualitatively different [20]. A Gaussian white noise $\xi_j(t)$ for each node was added with the standard deviation $\beta = 1$. We numerically solved the differential equations of the Stuart-Landau model using the 4th order Runge-Kutta method with 1,000 discretization steps. The first 5 seconds of time series were discarded and last 15 seconds were used for the analysis at each simulation. Therefore, each brain region generates its own spontaneous oscillatory dynamics near alpha bandwidth at each coupling strength K for one simulation.

Three brain states: below, near, and above critical State

We selected three representative brain states at different coupling strengths based on the level of global synchronization and the metastability to understand the responsiveness of different systems. We first calculated an order parameter $r(t)$ to obtain the level of global synchronization at time t using phase difference $\Delta\theta_{jk}(t) = \theta_j(t) - \theta_k(t)$ at each coupling strength K.

$$r(t) = \left\langle \left| \frac{1}{N} \sum_{k=1}^{N} A_{jk} e^{i\Delta\theta_{jk}(t)} \right| \right\rangle \quad (2)$$

Here $\mathrm{r(t)} = 1$ if all phases are equal, but $\mathrm{r(t)}$ is nearly zero if all phases are randomly distributed each other. Then we calculated the variance of $\mathrm{r(t)}$ for each coupling strength as a metastability to define the critical state $\mathrm{C_p}$ [25]. We considered that generated signals at certain coupling strength with the largest metastability can be equivalent to the spontaneous alpha oscillations in normal brain. There have been emerging evidences in computational model studies that the brain dynamics at critical point show the largest spatiotemporal diversity [29,51]. Notably, a large repertoire of metastable states exists in brain dynamics during conscious state [48]. With the critical state, we selected two other representative states which are below ($\mathrm{C_b}$) and above (C_a) critical states. We defined the $\mathrm{C_b}$ and $\mathrm{C_a}$ as the states with 10% and 90% percentile values of averaged order parameters over all coupling strengths, respectively. These states are the representative states far from the critical states which show small metastability. Generated signals in these three states were used for the analysis. We used 20 different initial frequency distributions and selected three representative states for each frequency distribution.

Brain network stimulation procedure

The global pulsatile stimuli were induced as a stimulation with $\mathrm{u(t)}$ as following:

$$\dot{z}_j(t) = \{\lambda_j + i\omega_j - |z_j(t)|^2\}z_j(t) + A_{ij}\sum_{k=1}^{N} K_{jk}z_k(t) - \tau_{jk} + \beta\xi_j(t) + u(t) \qquad (3)$$

$$u(t) = \begin{cases} p, & t_1 < t < t_2 \\ 0, & otherwise \end{cases} \qquad (4)$$

Here p is a strength of the stimulus during period $\mathrm{T} = \mathrm{t_2} - t_1$. We fixed the $\mathrm{p} = 30$ for the analysis after testing the effect of various stimulus strengths (S1 Fig.). We also fixed the duration of stimulus, $\mathrm{T} = 50\ \mathrm{msec}$ which is about a half of the period of cycle within alpha frequency range. We tested the stimulus duration from 50 msec to 250 msec (S2 Fig.). We gave a same stimulus to whole brain network to understand the dependence of response only derived from the network

534 dynamics of the system. The stimuli were induced at randomly selected timing t_1 for one trial.
535 Total 25 different timings were selected for each different frequency distribution with 10 iterations.
536 Therefore, C_b, C_p, and C_a have 500 stimulation trials with 500 different instantaneous brain states,
537 respectively. We decomposed the instantaneous brain states into the level of instantaneous
538 global synchronization, amplitude and phase of alpha waves to identify the relationship with the
539 responsiveness.

540 **Determining significant changes of amplitude and phase synchronization**

541 We assumed that the responses of amplitude and phase dynamics to the stimulus are different
542 in the system. Therefore, we investigated the perturbation response after the stimulus dividing
543 into two parts, amplitude and phase synchronization. First, we calculated the instantaneous
544 amplitude of j_{th} node, $|z_j(t)|$ for each trial. The instantaneous amplitudes for j_{th} node of one trial
545 were normalized by the mean and standard deviation of the baseline amplitudes of j_{th} node (1
546 second before the stimulus onset for each iteration). We considered the one tail $(1-\alpha)*100^{th}$
547 quantile with $\alpha = 0.05$ as a significantly increased amplitude after the stimulus onset. An amplitude
548 response of j_{th} node at time t was defined in a binary fashion: $PR_j^{amp}(t) = 1$ for the significantly
549 increased amplitude of node j; $PR_j^{amp}(t) = 0$, otherwise. Same procedures were performed for the
550 phase synchronization. The instantaneous phase synchronization for j_{th} node at time t was
551 obtained by taking average of the pairwise synchronization between node j and node k at time t,

552 $$D_j(t) = \left|\frac{1}{N_j}\sum_{k=1}^{N} A_{jk} e^{i\Delta\theta_{jk}(t)}\right| \qquad (5)$$

553 Here N_j is the number of connections of j_{th} node. A synchronization response after the stimulus
554 onset was also defined in a binary fashion: $PR_j^{sync}(t) = 1$ for the significantly increased phase
555 synchronization value; $PR_j^{sync}(t) = 0$, otherwise.

Responsiveness measures: Responsivity & Perturbational Complexity

We defined two different measures to quantify the responsiveness of different instantaneous brain states to the stimulus. First, the amplitude responsivity $\mathrm{R}^{amp}_{\mathrm{j}}$ and the synchronization responsivity $\mathrm{R}^{sync}_{\mathrm{j}}$ were defined by taking average of the perturbation response $\mathrm{PR}^{amp}_{\mathrm{j}}$ and $\mathrm{PR}^{sync}_{\mathrm{j}}$ of node j during specific time duration $\mathrm{t_{amp}}$ ($\mathrm{t_{sync}}$). It quantifies a total amount of significant perturbation responses after the stimulus onset. Here we used $\mathrm{t_{amp}}$= 600 msec and $\mathrm{t_{sync}}$= 200 msec, which covers the maximum response changes after the stimulus onset.

Second, we also calculated the Lempel-Ziv complexity (LZc) of the perturbation response for both amplitude and phase synchronization to understand how much information is contained in the response. LZc of the perturbation response for node j was defined as following:

$$\mathrm{LZc}^{amp}_{\mathrm{j}} = \frac{c^{amp}_{j}}{t_{amp}/\log_2 t_{amp}} \qquad (6)$$

$$\mathrm{LZc}^{sync}_{\mathrm{j}} = \frac{c^{sync}_{j}}{t_{sync}/\log_2 t_{sync}} \qquad (7)$$

Here $\mathrm{c}^{amp}_{\mathrm{j}}$ ($\mathrm{c}^{sync}_{\mathrm{j}}$) is the non-normalized Lempel-Ziv complexity of $\mathrm{PR}^{amp}_{\mathrm{j}}$ ($\mathrm{PR}^{sync}_{\mathrm{j}}$) calculated by a LZ76-algorithm [36], i.e., the number of unique patterns in the $\mathrm{PR}^{amp}_{\mathrm{j}}$ ($\mathrm{PR}^{sync}_{\mathrm{j}}$) during time $\mathrm{t_{amp}}$ ($\mathrm{t_{sync}}$). We defined a perturbational complexity, $\mathrm{LZc}^{amp}_{\mathrm{j}}$ ($\mathrm{LZc}^{sync}_{\mathrm{j}}$) as the normalized $\mathrm{c}^{\mathrm{amp}}_{\mathrm{j}}$ ($\mathrm{c}^{sync}_{\mathrm{j}}$).

We first investigated the relationships between the level of instantaneous global synchronization $\mathrm{r(t)}$ and the average R and LZc over all nodes at $\mathrm{C_b}$, $\mathrm{C_p}$, and $\mathrm{C_a}$. A Spearman correlation with p-value was calculated between the $\mathrm{r(t)}$ and the average R and LZc at $\mathrm{C_b}$, $\mathrm{C_p}$, and $\mathrm{C_a}$.

We also examined the instantaneous alpha amplitude/phase dependences of responsiveness ($\mathrm{R^{amp}}$, R^{sync}, LZc^{amp}, and LZc^{sync}) to the stimulus. Here we found the certain ongoing brain states of alpha oscillations that can induce large or small responsiveness at $\mathrm{C_p}$. We considered the

ongoing brain states with certain levels of instantaneous global synchronization, amplitudes, and phases inducing large (small) responsiveness as effective (non-effective) stimulation conditions and applied these conditions to stimulate the local areas described below.

Local stimulation effect

Next, we induced a stimulus to the left cuneus with regions within 50 mm radius in occipital region at C_p (13 regions; (left) cuneus, inferior parietal, isthmus cingulate, lateral occipital, lingual, pericalcarine, precuneus, superior parietal, (right) cuneus, isthmus cingulate, lingual, pericalcarine, precuneus) to confirm that the specific stimulation conditions we found from the global stimulation can be applied to the local stimulation. We selected the occipital region because abundant previous sensory stimulation studies mostly targeted the occipital region for visual tasks within alpha band. We compared the responsiveness measures, R^{amp}, R^{sync}, LZc^{amp} and LZc^{sync} with effective, non-effective and random stimulation conditions. For the effective (non-effective) stimulation, we applied the stimulus to the alpha phases from 240° to 360° (60° to 180°) with low (high) level of instantaneous global synchronization and low (high) amplitude. The stimulus was applied at random instantaneous states for the random stimulation condition. The stimulus was applied to random instantaneous brain states of occipital region for the random stimulation. The number of nodes for random stimulation was determined by a mean value of the number of nodes for effective and non-effective conditions. We performed 500 different trials at C_p, in which each trial consists of the stimuli with $p = 300$ for 50 msec at random timing t_1, and classified the nodes with specific conditions. We used Kruskal-Wallis test to compare significant difference among responsiveness of three conditions. Multiple comparison test was also performed (*p<0.05 and ***p<0.001).

Acknowledgments

This work is supported by grant No. R01 GM098578 (PIs: GM and UL) from the National Institutes of Health. We are grateful to Justin Campbell for his proofreading.

Reference

1. Ferrarelli F, Massimini M, Sarasso S, Casali A, Riedner BA, Angelini G, et al. Breakdown in cortical effective connectivity during midazolam-induced loss of consciousness. Proc Natl Acad Sci. 2010;107: 2681–2686. doi:10.1073/pnas.0913008107

2. Casali AG, Gosseries O, Rosanova M, Boly M, Sarasso S, Casali KR, et al. A theoretically based index of consciousness independent of sensory processing and behavior. Sci Transl Med. 2013;5. doi:10.1126/scitranslmed.3006294

3. Sarasso S, Rosanova M, Casali AG, Casarotto S, Fecchio M, Boly M, et al. Quantifying cortical EEG responses to TMS in (Un)consciousness. Clin EEG Neurosci. 2014;45: 40–49. doi:10.1177/1550059413513723

4. Sarasso S, Boly M, Napolitani M, Gosseries O, Charland-Verville V, Casarotto S, et al. Consciousness and complexity during unresponsiveness induced by propofol, xenon, and ketamine. Curr Biol. Elsevier; 2015;25: 3099–3105. doi:10.1016/j.cub.2015.10.014

5. Nunn CM, Osselton JW. The influence of the EEG alpha rhythm on the perception of visual stimuli. Psychophysiology. 1974. pp. 294–303.

6. Ergenoglu T, Demiralp T, Bayraktaroglu Z, Ergen M, Beydagi H, Uresin Y. Alpha rhythm of the EEG modulates visual detection performance in humans. Cogn Brain Res. 2004;20: 376–383. doi:10.1016/j.cogbrainres.2004.03.009

621 7. Romei V, Brodbeck V, Michel C, Amedi A, Pascual-Leone A, Thut G. Spontaneous
622 fluctuations in posterior α-band EEG activity reflect variability in excitability of human visual
623 areas. Cereb Cortex. 2008;18: 2010–2018. doi:10.1093/cercor/bhm229

624 8. van Dijk H, Schoffelen J-M, Oostenveld R, Jensen O. Prestimulus Oscillatory Activity in the
625 Alpha Band Predicts Visual Discrimination Ability. J Neurosci. 2008;28: 1816–1823.
626 doi:10.1523/JNEUROSCI.1853-07.2008

627 9. Busch NA, Dubois J, VanRullen R. The Phase of Ongoing EEG Oscillations Predicts Visual
628 Perception. J Neurosci. 2009;29: 7869–7876. doi:10.1523/JNEUROSCI.0113-09.2009

629 10. Mathewson KE, Gratton G, Fabiani M, Beck DM, Ro T. To See or Not to See:
630 Prestimulus Phase Predicts Visual Awareness. J Neurosci. 2009;29: 2725–2732.
631 doi:10.1523/JNEUROSCI.3963-08.2009

632 11. Mathewson KE, Lleras A, Beck DM, Fabiani M, Ro T, Gratton G. Pulsed out of awareness:
633 EEG alpha oscillations represent a pulsed-inhibition of ongoing cortical processing. Front
634 Psychol. 2011;2: 1–15. doi:10.3389/fpsyg.2011.00099

635 12. Dugue L, Marque P, VanRullen R. The Phase of Ongoing Oscillations Mediates the Causal
636 Relation between Brain Excitation and Visual Perception. J Neurosci. 2011;31: 11889–
637 11893. doi:10.1523/JNEUROSCI.1161-11.2011

638 13. Milton A, Pleydell-Pearce CW. The phase of pre-stimulus alpha oscillations influences the
639 visual perception of stimulus timing. Neuroimage. The Authors; 2016;133: 53–61.
640 doi:10.1016/j.neuroimage.2016.02.065

641 14. Benedetto A, Diego L-S, VanRullen R. 2017, Benedetto_et_al, Different responses of
642 spontaneous and stimulus-related alpha activity to ambient luminance changes.pdf.

643 15. Zrenner C, Desideri D, Belardinelli P, Ziemann U. Real-time EEG-defined excitability states

644 determine efficacy of TMS-induced plasticity in human motor cortex. Brain Stimul. Elsevier
645 Ltd; 2017;11: 374–389. doi:10.1016/j.brs.2017.11.016

646 16. Schaworonkow N, Triesch J, Ziemann U, Zrenner C. EEG-triggered TMS reveals stronger
647 brain state-dependent modulation of motor evoked potentials at weaker stimulation
648 intensities. bioRxiv. 2018; doi:10.1101/251363

649 17. Deco G, Cabral J, Saenger VM, Boly M, Tagliazucchi E, Laufs H, et al. Perturbation of
650 whole-brain dynamics in silico reveals mechanistic differences between brain states.
651 Neuroimage. Elsevier Ltd; 2018;169: 46–56. doi:10.1016/j.neuroimage.2017.12.009

652 18. Deco G, Cabral J, Woolrich MW, Stevner ABA, van Hartevelt TJ, Kringelbach ML. Single
653 or multiple frequency generators in on-going brain activity: A mechanistic whole-brain
654 model of empirical MEG data. Neuroimage. Elsevier; 2017;152: 538–550.
655 doi:10.1016/j.neuroimage.2017.03.023

656 19. Jobst BM, Hindriks R, Laufs H, Tagliazucchi E, Hahn G, Ponce-Alvarez A, et al. Increased
657 Stability and Breakdown of Brain Effective Connectivity during Slow-Wave Sleep:
658 Mechanistic Insights from Whole-Brain Computational Modelling. Sci Rep. 2017;7: 1–16.
659 doi:10.1038/s41598-017-04522-x

660 20. Moon JY, Lee UC, Blain-Moraes S, Mashour GA. General relationship of global topology,
661 local dynamics, and directionality in large-scale brain networks. PLoS Comput Biol.
662 2015;11: 1–21. doi:10.1371/journal.pcbi.1004225

663 21. Moon JY, Kim J, Ko TW, Kim M, Iturria-Medina Y, Choi JH, et al. Structure shapes
664 dynamics and directionality in diverse brain networks: Mathematical principles and
665 empirical confirmation in three species. Sci Rep. 2017; doi:10.1038/srep46606

666 22. Kim M, Kim S, Mashour GA, Lee U. Relationship of Topology, Multiscale Phase

Synchronization, and State Transitions in Human Brain Networks. Front Comput Neurosci. 2017;11: 1–12. doi:10.3389/fncom.2017.00055

23. Zhang H, Watrous AJ, Patel A, Jacobs J. Theta and Alpha Oscillations Are Traveling Waves in the Human Neocortex. Neuron. Elsevier; 2018;98: 1269–1281.e4. doi:10.1016/j.neuron.2018.05.019

24. Kim H, Moon J, Mashour GA, Lee U. Mechanisms of hysteresis in human brain networks during transitions of consciousness and unconsciousness : Theoretical principles and empirical evidence. 2018; 1–22.

25. Shanahan M. Metastable chimera states in community-structured oscillator networks. Chaos An Interdiscip J Nonlinear Sci. 2010;20: 013108. doi:10.1063/1.3305451

26. Chialvo DR. Emergent complex neural dynamics. Nat Phys. Nature Publishing Group; 2010;6: 744–750. doi:10.1038/nphys1803

27. Cocchi L, Gollo LL, Zalesky A, Breakspear M. Criticality in the brain: A synthesis of neurobiology, models and cognition. Prog Neurobiol. Elsevier Ltd; 2017;158: 132–152. doi:10.1016/j.pneurobio.2017.07.002

28. Kitzbichler MG, Smith ML, Christensen SR, Bullmore E. Broadband criticality of human brain network synchronization. PLoS Comput Biol. 2009;5. doi:10.1371/journal.pcbi.1000314

29. Haimovici A, Tagliazucchi E, Balenzuela P, Chialvo DR. Brain organization into resting state networks emerges at criticality on a model of the human connectome. Phys Rev Lett. 2013;110: 1–4. doi:10.1103/PhysRevLett.110.178101

30. Hutt A, Lefebvre J, Hight D, Sleigh J. Suppression of underlying neuronal fluctuations mediates EEG slowing during general anaesthesia. Neuroimage. 2018;179: 414–428.

690 doi:10.1016/j.neuroimage.2018.06.043

691 31. VanRullen R, Koch C. Is perception discrete or continuous? Trends Cogn Sci. 2003;7: 207–
692 213. doi:10.1016/S1364-6613(03)00095-0

693 32. VanRullen R. Perceptual Cycles. Trends Cogn Sci. Elsevier Ltd; 2016;20: 723–735.
694 doi:10.1016/j.tics.2016.07.006

695 33. VanRullen R. Attention Cycles. Neuron. Elsevier Inc.; 2018;99: 632–634.
696 doi:10.1016/j.neuron.2018.08.006

697 34. Callaway E, Alexander JD. The temporal coding of sensory data: An investigation of two
698 theories. J Gen Psychol. 1960;62: 293–309. doi:10.1080/00221309.1960.9920419

699 35. Daffertshofer A, Ton R, Kringelbach ML, Woolrich M, Deco G. Distinct criticality of phase
700 and amplitude dynamics in the resting brain. Neuroimage. Elsevier Ltd; 2018; 1–6.
701 doi:10.1016/j.neuroimage.2018.03.002

702 36. Lempel A, Ziv J. On the complexity of finite sequences IEEE Transactions on Information
703 Theory Vol IT22. IEEE Trans Inf Theory1. 1976;22: 75–81. doi:10.1109/TIT.1976.1055501

704 37. Fekete T, Omer DB, O'Hashi K, Grinvald A, van Leeuwen C, Shriki O. Critical dynamics,
705 anesthesia and information integration: Lessons from multi-scale criticality analysis of
706 voltage imaging data. Neuroimage. Elsevier Inc.; 2018;183: 919–933.
707 doi:10.1016/j.neuroimage.2018.08.026

708 38. Brüers S, VanRullen R. Alpha power modulates perception independently of endogenous
709 factors. Front Neurosci. 2018;12: 1–8. doi:10.3389/fnins.2018.00279

710 39. Samaha J, Gosseries O, Postle BR. Distinct Oscillatory Frequencies Underlie Excitability
711 of Human Occipital and Parietal Cortex. J Neurosci. 2017;37: 2824–2833.

doi:10.1523/JNEUROSCI.3413-16.2017

40. Huang Z, Zhang J, Longtin A, Dumont G, Duncan NW, Pokorny J, et al. Is There a Nonadditive Interaction Between Spontaneous and Evoked Activity? Phase-Dependence and Its Relation to the Temporal Structure of Scale-Free Brain Activity. Cereb Cortex. 2017;27: 1037–1059. doi:10.1093/cercor/bhv288

41. Harris KD, Thiele A. Cortical state and attention. Nat Rev Neurosci. Nature Publishing Group; 2011;12: 509–523. doi:10.1038/nrn3084

42. Cecere R, Rees G, Romei V. Individual differences in alpha frequency drive crossmodal illusory perception. Curr Biol. The Authors; 2015;25: 231–235. doi:10.1016/j.cub.2014.11.034

43. Zerlaut Y, Destexhe A. Enhanced Responsiveness and Low-Level Awareness in Stochastic Network States. Neuron. Elsevier Inc.; 2017;94: 1002–1009. doi:10.1016/j.neuron.2017.04.001

44. Granada A, Hennig RM, Ronacher B, Kramer A, Herzel H. Phase response curves elucidating the dynamics of coupled oscillators. Methods Enzymol. 2009;454: 1–27. doi:10.1016/S0076-6879(08)03801-9

45. Hannay KM, Booth V, Forger DB. Collective phase response curves for heterogeneous coupled oscillators. Phys Rev E - Stat Nonlinear, Soft Matter Phys. 2015;92: 1–9. doi:10.1103/PhysRevE.92.022923

46. Ko T-W, Ermentrout B. Phase Response Curves of Coupled Oscillators. 2008; 1–6. doi:10.1103/PhysRevE.79.016211

47. Levnajić Z, Pikovsky A. Phase resetting of collective rhythm in ensembles of oscillators. Phys Rev E - Stat Nonlinear, Soft Matter Phys. 2010;82: 1–10.

735 doi:10.1103/PhysRevE.82.056202

736 48. Deco G, Kringelbach ML, Jirsa VK, Ritter P. The dynamics of resting fluctuations in the
737 brain: Metastability and its dynamical cortical core. Sci Rep. Springer US; 2017;7: 1–14.
738 doi:10.1038/s41598-017-03073-5

739 49. van den Heuvel MP, Sporns O. Rich-Club Organization of the Human Connectome. J
740 Neurosci. 2011;31: 15775–15786. doi:10.1523/JNEUROSCI.3539-11.2011

741 50. Caminiti R, Carducci F, Piervincenzi C, Battaglia-Mayer A, Confalone G, Visco-Comandini
742 F, et al. Diameter, Length, Speed, and Conduction Delay of Callosal Axons in Macaque
743 Monkeys and Humans: Comparing Data from Histology and Magnetic Resonance Imaging
744 Diffusion Tractography. J Neurosci. 2013;33: 14501–14511.
745 doi:10.1523/JNEUROSCI.0761-13.2013

746 51. Hudetz AG, Humphries CJ, Binder JR. Spin-glass model predicts metastable brain states
747 that diminish in anesthesia. Front Syst Neurosci. 2014;8: 1–9.
748 doi:10.3389/fnsys.2014.00234

749

750

751

752 ## Supporting information

753

754 **S1 Fig. Average (A) PR^{amp} and (B) PR^{sync} over all trials with respect to the strength of the**
755 **pulsatile stimuli p.** The error bar indicates a standard deviation. Both PR^{amp} and PR^{sync} are
756 increased when p is increased.

S2 Fig. (Left panel) PR^{amp} and (Right panel) PR^{sync} of one trial with different durations of stimuli with the strength $p = 30$. The stimulus duration was varied from 50 to 250 msec with 50 msec intervals. Red rectangle indicates the duration of stimulus.

S3 Fig. Average perturbational complexity of (A) amplitude (LZc^{amp}) and (B) phase synchronization (LZc^{sync}) at C_b, C_p, and C_a. Kruskal-Wallis test was performed (***p<0.001 for both amplitude and phase synchronization LZc). Multi-comparison test was also performed using Tukey-Kramer method (***p<0.001).

S4 Fig. Alpha phase dependence of responsiveness at C_p (See Fig 6 in the main text). For each panel, a red (blue) thick line indicates the average (A) R^{amp}, (B) R^{sync}, (C) LZc^{amp}, (D) LZc^{sync} of nodes with lower (higher) level of instantaneous global synchronization and lower (higher) amplitude at the stimulus onset. Lower and higher levels of instantaneous global synchronization (amplitude) were distinguished by the average of instantaneous global synchronization levels of all trials (amplitudes of all nodes). Phases of nodes at the stimulus onset were sorted in 30 phase bins. Thin lines indicate the standard errors of responsiveness.4 different conditions were classified; LS & LA (red), LS & HA (orange), HS & LA (light blue), and HS & HA (blue).

S5 Fig. Alpha phase dependence of responsiveness at C_p for the stimuli strength $p = 10$. For each panel, a red (blue) thick line indicates the average (A) R^{amp}, (B) R^{sync}, (C) LZc^{amp}, (D) LZc^{sync} of nodes with lower (higher) level of instantaneous global synchronization and lower (higher) amplitude at the stimulus onset. Lower and higher levels of instantaneous global synchronization (amplitude) were distinguished by the average of instantaneous global synchronization levels of all trials (amplitudes of all nodes). Phases of nodes at the stimulus onset were sorted in 30 phase bins. Thin lines indicate the standard errors of responsiveness.4 different conditions were classified; LS & LA (red), LS & HA (orange), HS & LA (light blue), and HS & HA (blue). Responsiveness is small for all measures.

S6 Fig. Alpha phase dependence of responsiveness at C_p for the stimuli strength $p = 20$. For each panel, a red (blue) thick line indicates the average (A) R^{amp}, (B) R^{sync}, (C) LZc^{amp}, (D) LZc^{sync} of nodes with lower (higher) level of instantaneous global synchronization and lower (higher) amplitude at the stimulus onset. Lower and higher levels of instantaneous global synchronization (amplitude) were distinguished by the average of instantaneous global synchronization levels of all trials (amplitudes of all nodes). Phases of nodes at the stimulus onset were sorted in 30 phase bins. Thin lines indicate the standard errors of responsiveness.4 different conditions were classified; LS & LA (red), LS & HA (orange), HS & LA (light blue), and HS & HA (blue). The responsiveness curves are similar with the responsiveness curve with the strength $p = 30$ except the LZc^{amp}.

S7 Fig. Alpha phase dependence of responsiveness at C_p for the stimuli strength $p = 40$. For each panel, a red (blue) thick line indicates the average (A) R^{amp}, (B) R^{sync}, (C) LZc^{amp}, (D) LZc^{sync} of nodes with lower (higher) level of instantaneous global synchronization and lower (higher) amplitude at the stimulus onset. Lower and higher levels of instantaneous global synchronization (amplitude) were distinguished by the average of instantaneous global synchronization levels of all trials (amplitudes of all nodes). Phases of nodes at the stimulus onset were sorted in 30 phase bins. Thin lines indicate the standard errors of responsiveness. 4 different conditions were classified; LS & LA (red), LS & HA (orange), HS & LA (light blue), and HS & HA (blue). The responsiveness curves are similar with the responsiveness curve with the strength $p = 30$, but synchronization responsiveness measures, R^{sync} and LZc^{sync} are similar for all phase ranges.

S8 Fig. Alpha phase dependence of responsiveness at C_p for the stimuli strength $p = 50$. For each panel, a red (blue) thick line indicates the average (A) R^{amp}, (B) R^{sync}, (C) LZc^{amp}, (D) LZc^{sync} of nodes with lower (higher) level of instantaneous global synchronization and lower (higher) amplitude at the stimulus onset. Lower and higher levels of instantaneous global synchronization (amplitude) were distinguished by the average of instantaneous global synchronization levels of all trials (amplitudes of all nodes). Phases of nodes at the stimulus onset

were sorted in 30 phase bins. Thin lines indicate the standard errors of responsiveness. 4 different conditions were classified; LS & LA (red), LS & HA (orange), HS & LA (light blue), and HS & HA (blue). Lower amplitude shows larger amplitude responsiveness in (A) and (C), and lower synchronization shows larger synchronization responsiveness in (B) and (D).

S9 Fig. The instantaneous global synchronization level, node amplitude and phase dependences of responsivity $\boldsymbol{R}$ at $\boldsymbol{C_b}$, $\boldsymbol{C_p}$, and $\boldsymbol{C_a}$. (A) First, 100 trials stimulating at lower (left) / higher (right) levels of instantaneous global synchronization (Low synch and High synch, respectively) in C_b, C_p and C_a were selected. Dots indicate 5% of nodes with the largest (smallest) R^{amp} in one trial. Color of dots indicates the value of R^{amp} of the node. A distance from the origin is the instantaneous node amplitude, and a phase angle is the node phase at the stimulus onset. The phase is important to determine the R^{amp} at C_b. The phase ranges from 60° to 180° of the signal have smaller R^{amp} for all three states. (B) Same as (A), but a color of dots indicates the value of R^{sync} of the node. Nodes with lower amplitude tend to have larger R^{sync} in High synch at C_p. Nodes with lower amplitude tend to have larger R^{sync} in Low synch at C_a.

S10 Fig. The instantaneous global synchronization level, node amplitude and phase dependences of perturbational complexity $\boldsymbol{LZc}$ at $\boldsymbol{C_b}$, $\boldsymbol{C_p}$, and $\boldsymbol{C_a}$. (A) First, 100 trials stimulating at lower (left) / higher (right) levels of instantaneous global synchronization (Low synch and High synch, respectively) in C_b, C_p and C_a were selected. Dots indicate 5% of nodes with the largest (smallest) LZc^{amp} in one trial. Color of dots indicates the value of LZc^{amp} of the node. A distance from the origin is the instantaneous node amplitude, and a phase angle is the node phase at the stimulus onset. The ongoing phase dependence is shown in the LZc^{amp} at C_b. Nodes with lower amplitude tend to show larger LZc^{amp} at C_p in High synch. (B) Same as (A), but a color of dots indicates the value of LZc^{sync} of the node. Nodes with lower amplitude tend to have larger LZc^{sync} in High synch at C_p. Nodes with lower amplitude appeared to have larger R^{sync} in Low synch at C_a.

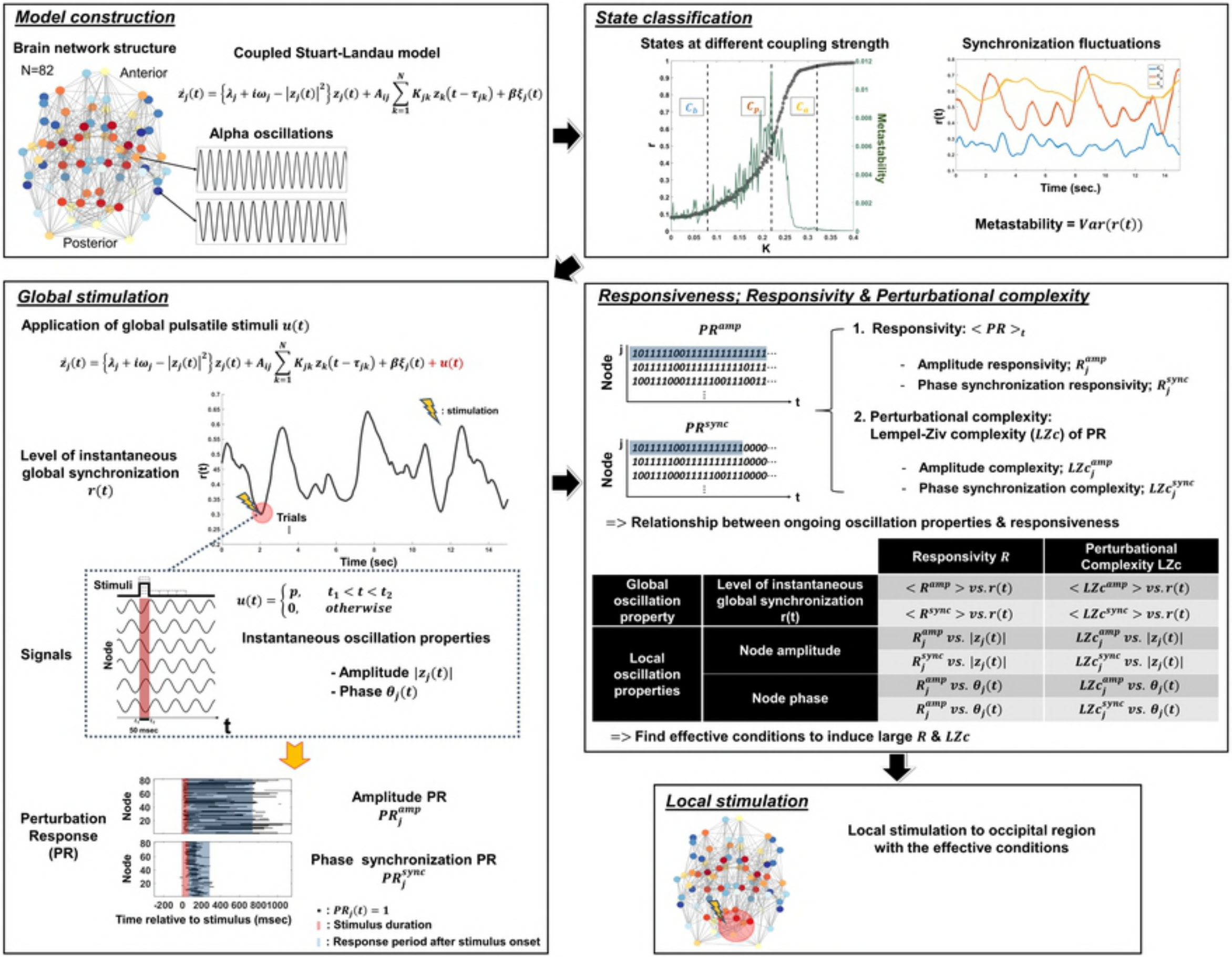
Model construction
Brain network structure
N=82
Anterior
Posterior
Coupled Stuart-Landau model
$\dot{z}_j(t) = \{\lambda_j + i\omega_j - |z_j(t)|^2\} z_j(t) + A_{ij} \sum_{k=1}^{N} K_{jk} z_k(t-\tau_{jk}) + \beta\xi_j(t)$
Alpha oscillations
State classification
States at different coupling strength
Synchronization fluctuations
Metastability
K
r(t)
Time (sec.)
Metastability = $Var(r(t))$
Global stimulation
Application of global pulsatile stimuli $u(t)$
$\dot{z}_j(t) = \{\lambda_j + i\omega_j - |z_j(t)|^2\} z_j(t) + A_{ij} \sum_{k=1}^{N} K_{jk} z_k(t-\tau_{jk}) + \beta\xi_j(t) + u(t)$
Level of instantaneous global synchronization $r(t)$
: stimulation
Trials
Time (sec)
Signals
Stimuli
Node
50 msec
$u(t) = \begin{cases} p, & t_1 < t < t_2 \\ 0, & otherwise \end{cases}$
Instantaneous oscillation properties
- Amplitude $|z_j(t)|$
- Phase $\theta_j(t)$
Perturbation Response (PR)
Amplitude PR PR_j^{amp}
Phase synchronization PR PR_j^{sync}
Time relative to stimulus (msec)
• : $PR_j(t) = 1$
: Stimulus duration
: Response period after stimulus onset
Responsiveness; Responsivity & Perturbational complexity
PR^{amp}
PR^{sync}
Node
1. Responsivity: $< PR >_t$
- Amplitude responsivity; R_j^{amp}
- Phase synchronization responsivity; R_j^{sync}
2. Perturbational complexity: Lempel-Ziv complexity (LZc) of PR
- Amplitude complexity; LZc_j^{amp}
- Phase synchronization complexity; LZc_j^{sync}
=> Relationship between ongoing oscillation properties & responsiveness
Responsivity R
Perturbational Complexity LZc
Global oscillation property
Level of instantaneous global synchronization r(t)
$< R^{amp} > vs. r(t)$
$< LZc^{amp} > vs. r(t)$
$< R^{sync} > vs. r(t)$
$< LZc^{sync} > vs. r(t)$
Local oscillation properties
Node amplitude
R_j^{amp} vs. $|z_j(t)|$
LZc_j^{amp} vs. $|z_j(t)|$
R_j^{sync} vs. $|z_j(t)|$
LZc_j^{sync} vs. $|z_j(t)|$
Node phase
R_j^{amp} vs. $\theta_j(t)$
LZc_j^{amp} vs. $\theta_j(t)$
R_j^{amp} vs. $\theta_j(t)$
LZc_j^{sync} vs. $\theta_j(t)$
=> Find effective conditions to induce large R & LZc
Local stimulation
Local stimulation to occipital region with the effective conditions

Figure 1

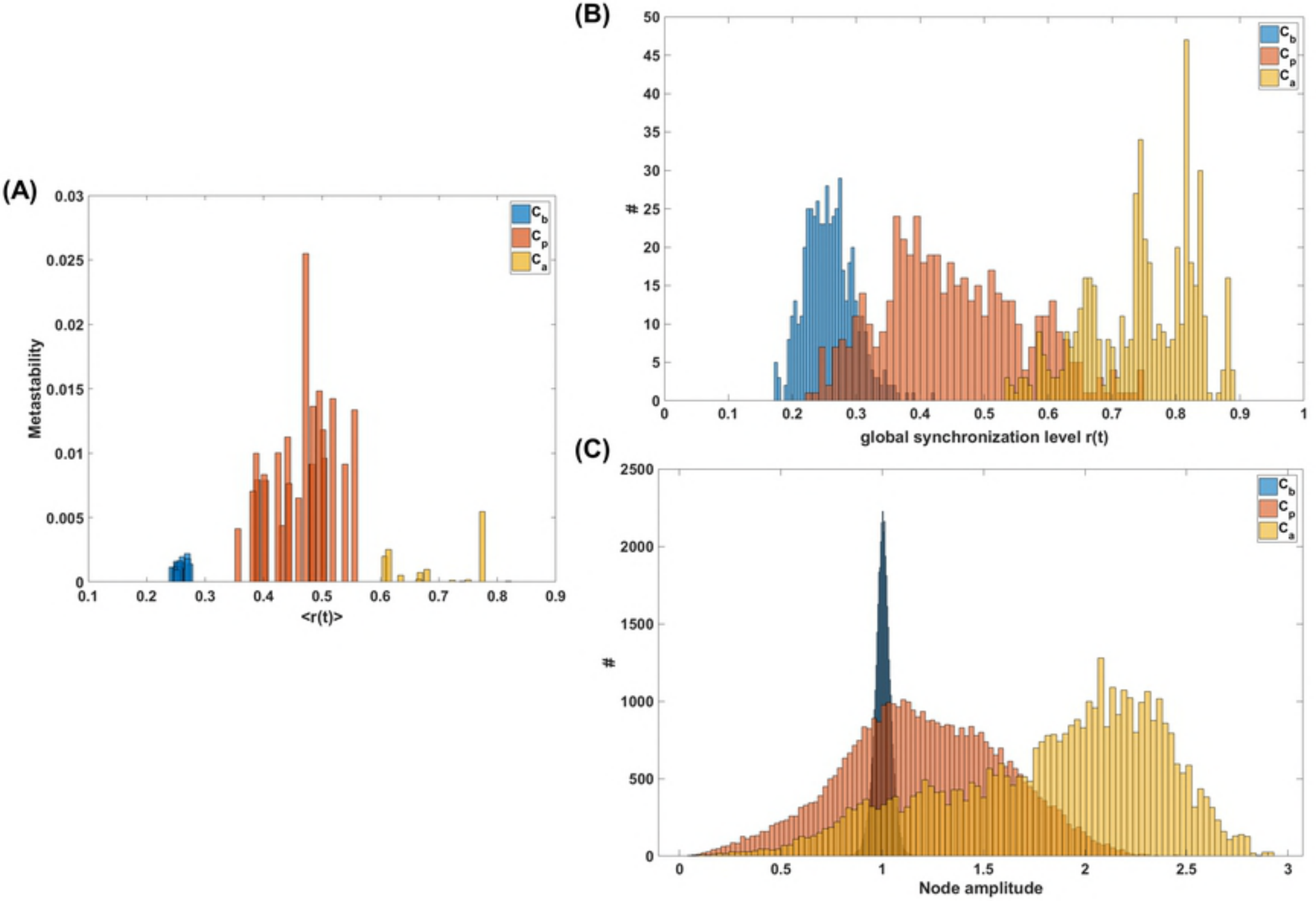
(A)
Metastability
<r(t)>
(B)
#
global synchronization level r(t)
(C)
#
Node amplitude
C_b
C_p
C_a

Figure 2

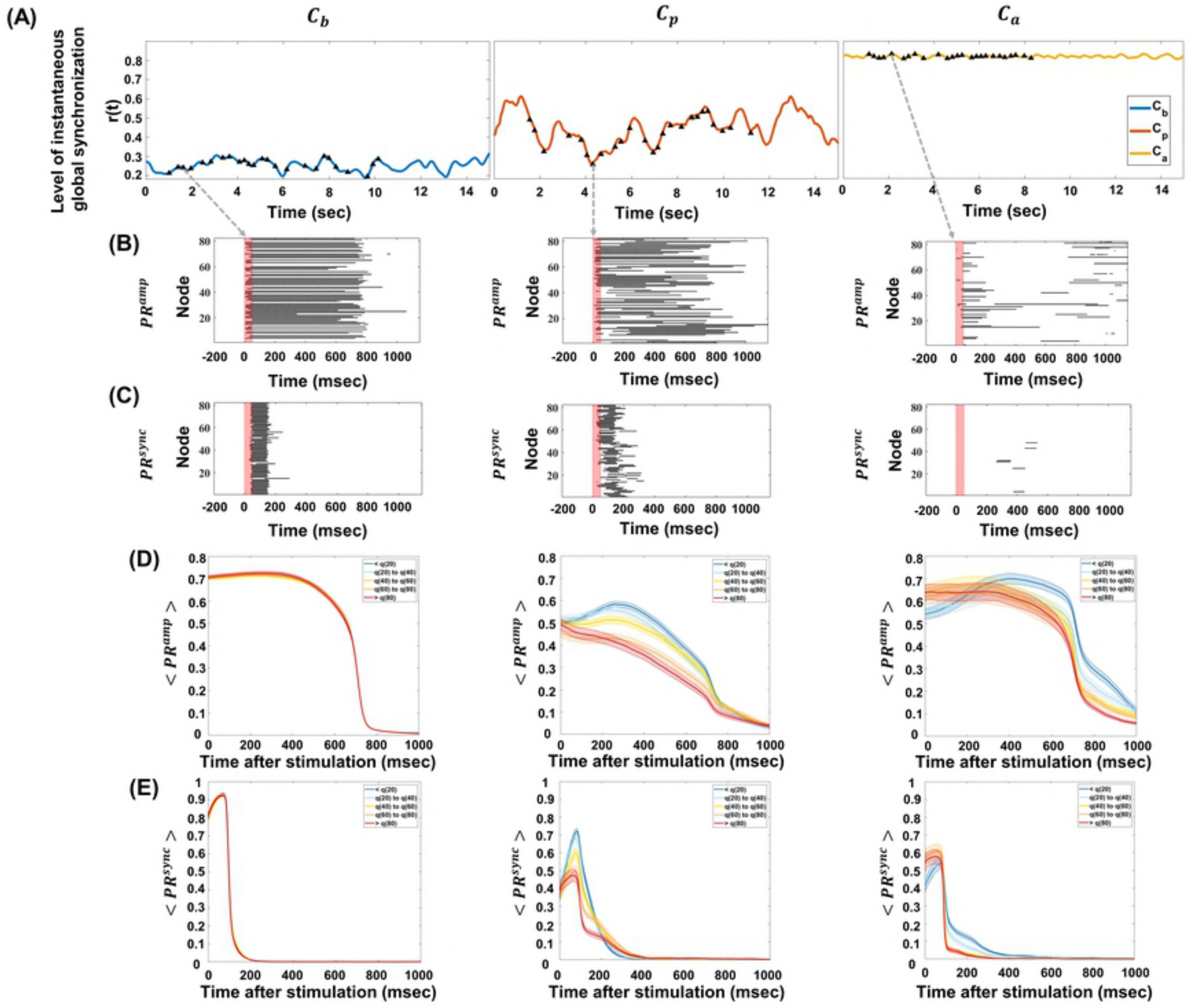
(A)
C_b
C_p
C_a
Level of instantaneous global synchronization
r(t)
Time (sec)
C_b
C_p
C_a
(B)
PR^{amp}
Node
Time (msec)
(C)
PR^{sync}
Node
Time (msec)
(D)
$< PR^{amp} >$
Time after stimulation (msec)
(E)
$< PR^{sync} >$
Time after stimulation (msec)

Figure 3

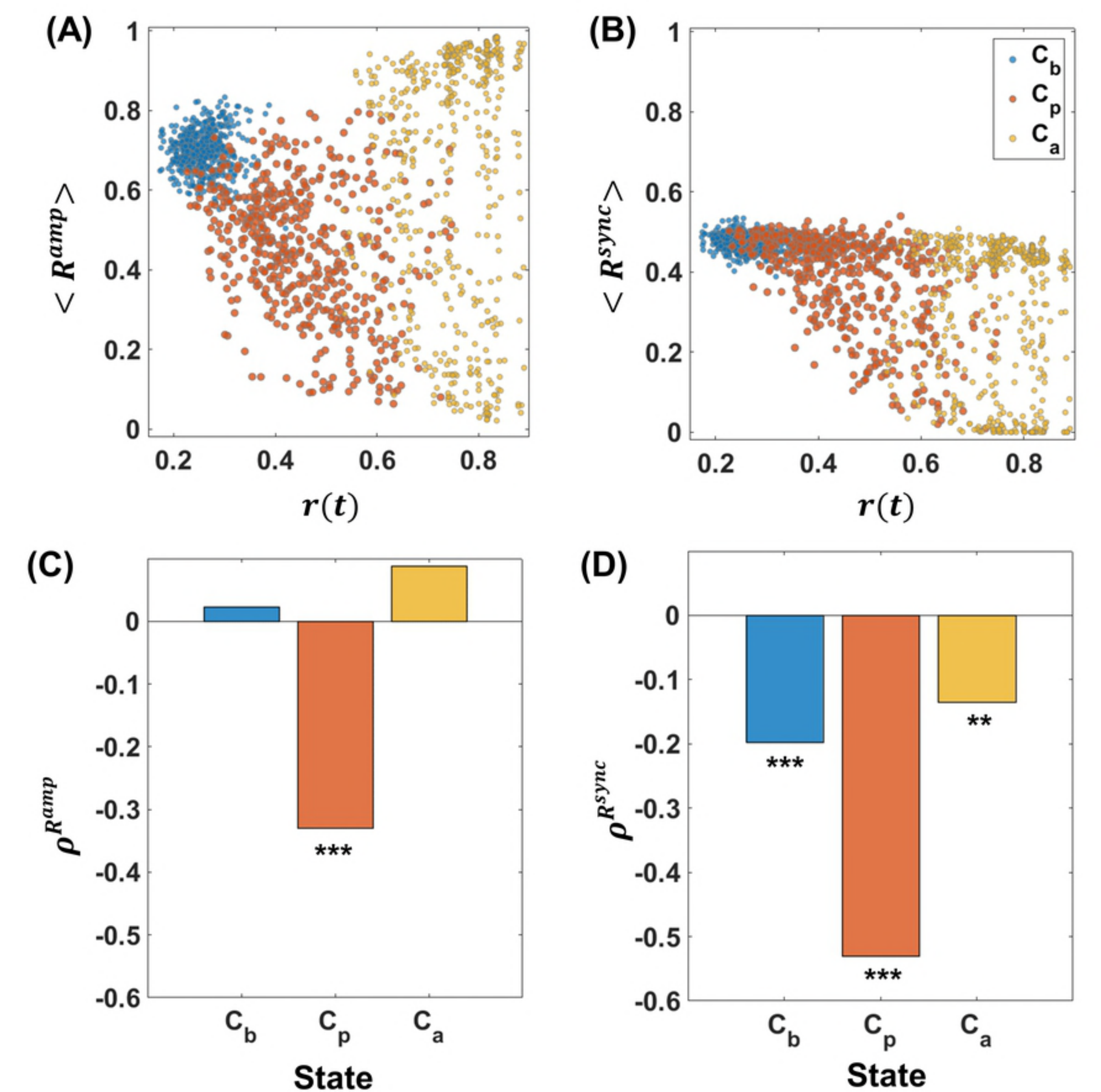

Figure 4

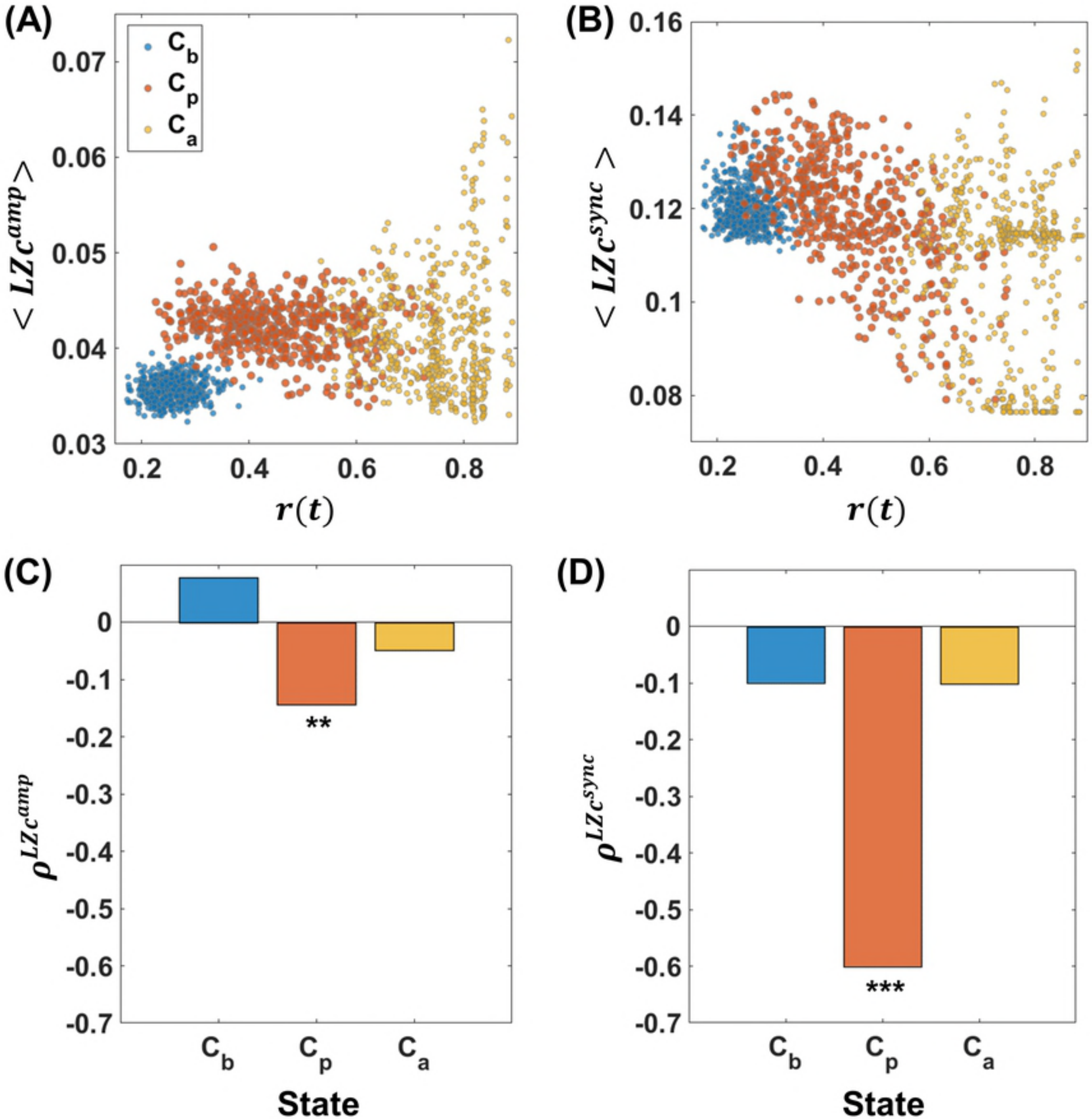

Figure 5

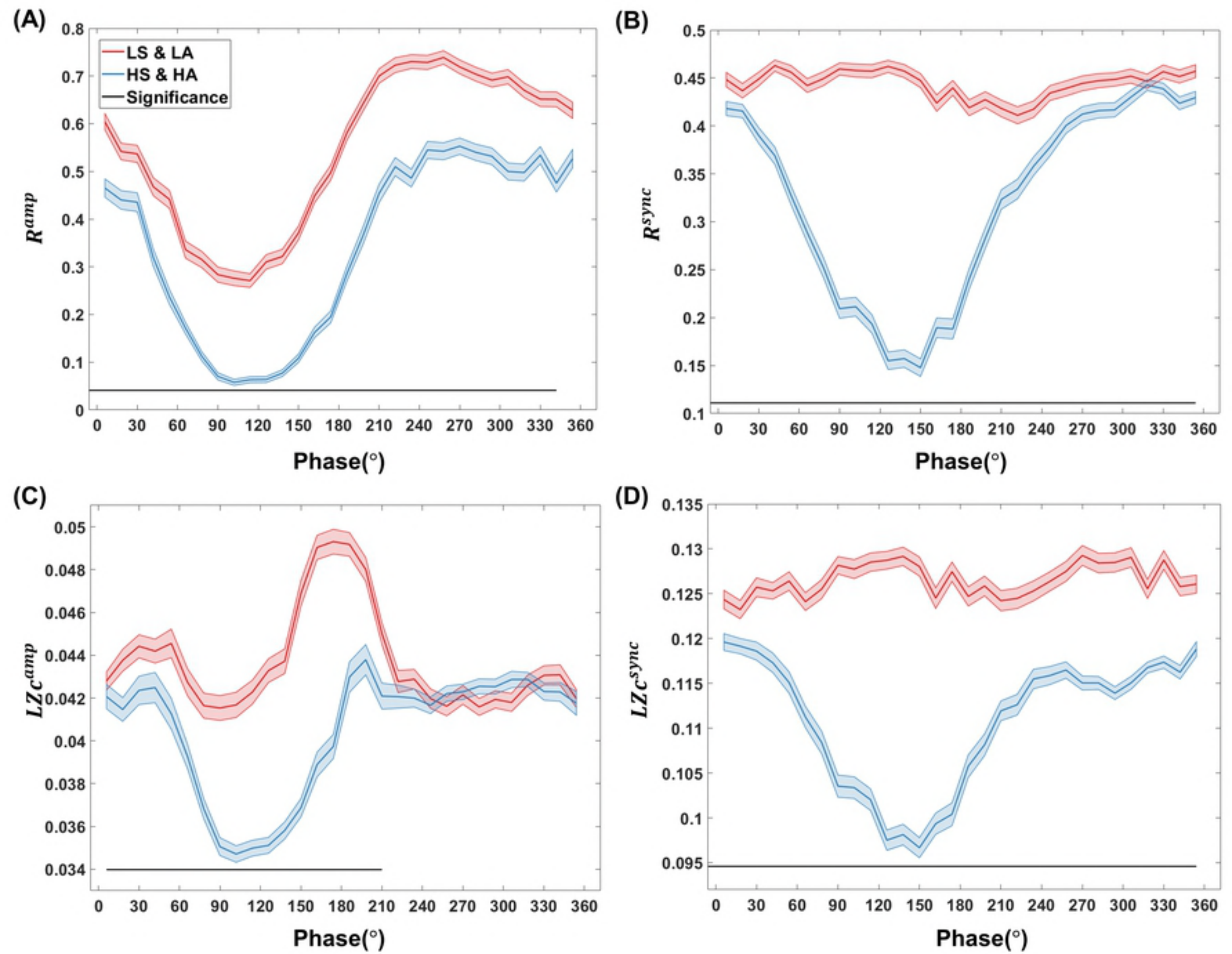
(A)
LS & LA
HS & HA
Significance
R^{amp}
Phase(°)
(B)
R^{sync}
Phase(°)
(C)
LZc^{amp}
Phase(°)
(D)
LZc^{sync}
Phase(°)

Figure 6

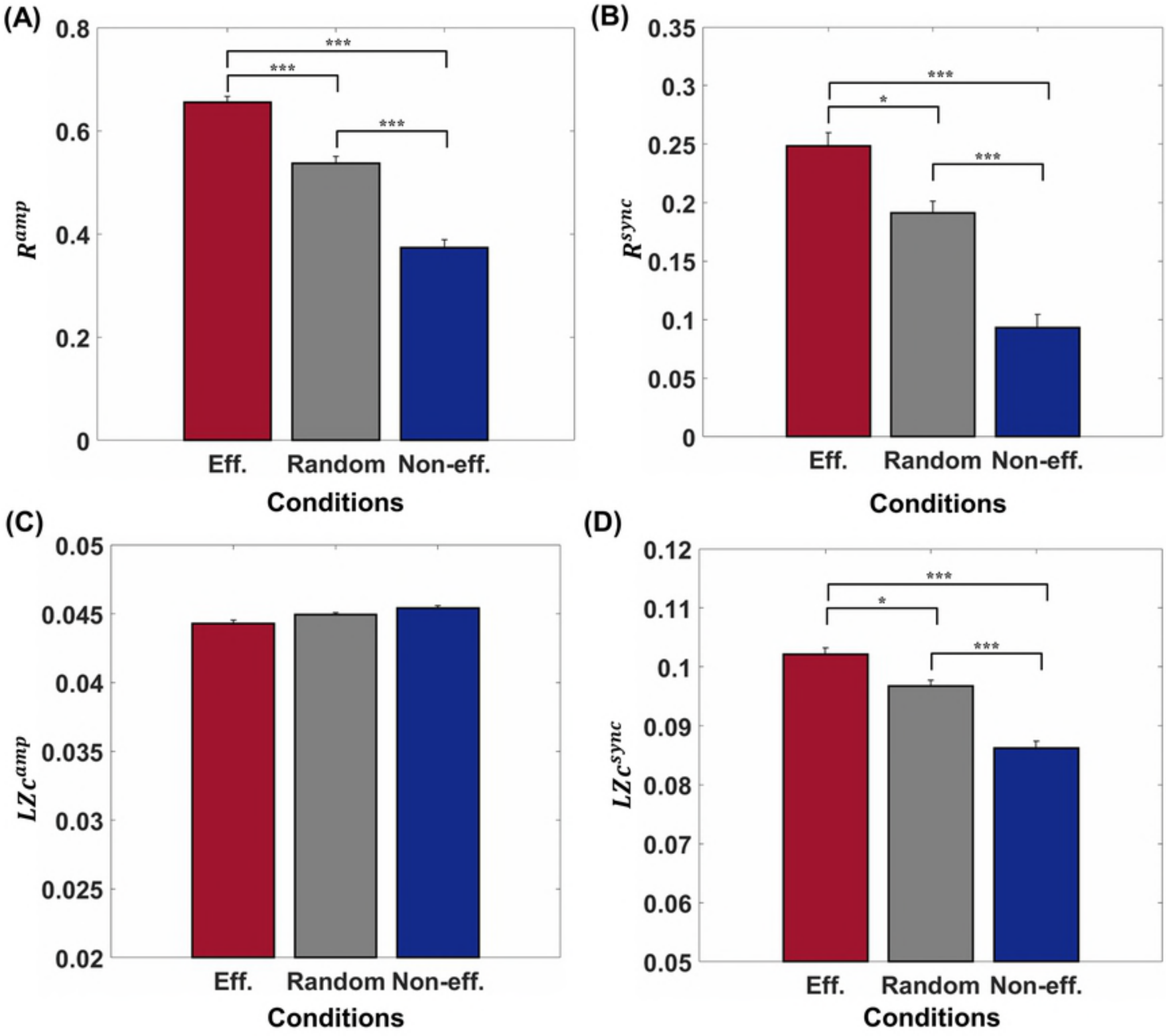
(A)
0.8
0.6
0.4
0.2
0
R^{amp}
***
***
***
Eff.
Random
Non-eff.
Conditions
(B)
0.35
0.3
0.25
0.2
0.15
0.1
0.05
0
R^{sync}
***
*
***
Eff.
Random
Non-eff.
Conditions
(C)
0.05
0.045
0.04
0.035
0.03
0.025
0.02
LZc^{amp}
Eff.
Random
Non-eff.
Conditions
(D)
0.12
0.11
0.1
0.09
0.08
0.07
0.06
0.05
LZc^{sync}
***
*
***
Eff.
Random
Non-eff.
Conditions

Figure 7